Journal of Metals, Materials and Minerals. Vol. 13 No. 1 pp. 7-15, 2003.

Synthesized nanocomposite TiN/*a*-SiN_x films

Natthapong PHINICHKA[1], Ramesh CHANDRA[2] and Zoe H. BARBER[3]

[1]Faculty of Science, Department of General Science, Srinakharinwirot University, Bangkok, Thailand
[2]Department of physics, Ch. Charan Singh University, Meerut, India
[3]Department of Materials Science and Metallurgy, University of Cambridge, UK

ABSTRACT

Nanocomposite hard coatings, *nc*-TiN/*a*-SiN_x, were synthesized by an ionized magnetron sputter deposition technique (IMSD). The maximum hardness of 40.06 GPa, approximately double that of TiN, is reached at $Ti_{0.88}$:$Si_{0.12}$ with an rf power of 100 W and negative bias of 150 V. The hardness of the films was measured using nanoindentation. At an applied load of less than 70 mN, the indentation depth is less than 10% of the film thickness and the results show no effect of substrate on the hardness of the films. The effects of ion flux and energetic bombardment on the properties of the films were observed by varying the rf power to the built-in rf coil where an inductively coupled plasma is generated, and the dc substrate bias of which the bombardment energy is controlled. X-ray diffraction was used to investigate the structure and grain size, and its correlation with hardness behavior as a function of Si content and bias voltage. Only one phase that can be assigned to TiN was found. No signals from crystalline Si_3N_4 or other phases of titanium silicide were observed. The preferential growth, as a function of Si content and bias voltage, changes from (111) to a preferred (200) orientation when negative bias voltage and Si content is increased. For high hardness films, the nanocrystallite domain size of the TiN, calculated from peak broadening, was found to be less than 10 nm.

*To whom the correspondence should be addressed:
E-mail address : Natthapong@swu.ac.th

INTRODUCTION

Today more than 40% of cutting tools are coated by wear resistant materials (Veprek, 1999). Due to their high hardness, 20 GPa, titanium nitride is widely used to improve the wear resistance and durability of the cutting tools. However, it is known that TiN starts to oxidize at low temperature, 500^{o}C (Jedrzejowski, *et al.* 2003). Therefore, in the past decade, efforts to search for materials that have high hardness, oxidation resistance, and chemical stability have been established.

Nanocomposite materials are materials that are prepared to have inhomogeneity on a smaller scale than the submicron scale, in which their grain size decreases to approximately 10 nm. This new generation of materials exhibits new physical and service properties because the interaction between grains has significantly changed. Nanocomposite coatings have recently attracted much interest because of their high hardness, wear resistance, and good thermal and chemical stability. The hardness of nanocomposite materials arises from the presence of nanometer scale grains, which hinders the generation and movement of dislocations, stops crack propagation due to the presence of grain boundaries, and suppresses grain boundary sliding (Kim, *et al.* 2002; and Musil, *et al.* 2001). This is in contrast to intrinsic superhard thin film materials, the hardness of which comes from the high strength of covalent interatomic bonds, short bond distances, and a high coordination number (Rebouta, *et al.* 2000; and Vaz, *et al.* 2000)

Nanocomposite coatings can be divided into three groups according to their hardness: Boulch, *et al*. (2001). Hard coatings with hardness H < 40 GPa; Chiu and Barber (2002), superhard coatings with 40 ≤ H ≤ 80 GPa; Chiu, *et al.* (1999) and ultrahard coatings with H > 80 GPa. (Niederhofer, *et al.* 1999). At present the two phases hard and superhard nanocomposite can be divided into two groups: Boulch, *et al*. (2001) *nc*-M_nN/hard phase; and Chiu and Barber (2002) *nc*-M_nN/soft phase. Where M is the element that can form hard nitride (e.g. W, Ti, Cr, Zr, V), hard phase is amorphous (e.g. *a*-Si_3N_4, *a*-TiB_2), and soft phase is soft metal (e.g. Cu, Ni, Ag) (Musil and Vlcek, 2001)**.** The ultrahard coating that has hardness >80 GPa consisteds of a nanocrystalline and two amorphous phases (e.g. *nc*-TiN/*a*-Si_3N_4/*a*-$TiSi_2$) and the one that has hardness ≥100 GPa consists of two nanocrystalline and amorphous phases (e.g. *nc*-TiN/*a*-Si_3N_4/*nc*-$TiSi_2$/*a*-$TiSi_2$) (Neiderhofer, *et al.* 2001).

One of the most studied hard and superhard two-phase nanocomposite coatings is *nc*-TiN/*a*-SiN*x* (Diserens, *et al*. 1998; Jedrzejowski; *et al.* 2003; Martin, *et al.* 2003; Meng, *et al.* 2003; Niederhofer, *et al.* 1999; Rebouta, *et al.* 2000; Veprek, 1999; and Zhang, *et al*. 2003). These nanocomposite films are composed of nanocrystalline TiN embedded in an amorphous silicon nitride matrix and have been synthesized by both plasma-assisted chemical vapor deposition (PACVD) and physical vapor deposition (PVD). The PACVD technique generates intense ion bombardment during film growth (Jedrzejowski, *et al.* 2003; and Veprek, 1999)**.** However, hazardous $TiCl_4$ and $SiCl_4$ or SiH_4 gases are required, and this leads to difficult safety and environmental issues (Jedrzejowski, *et al.* 2003; and Patsheider, *et al.* 1996)**.** A range of PVD techniques haves been used to prepare Ti-Si-N nanocomposite hard coatings, including RF and DC magnetron and unbalanced magnetron sputtering (Diserens, *et al*. 1998; Martin, *et al.* 2003; Rebouta, *et al.* 2000; and Zhang, *et al*. 2003). In general these techniques are cleaner and safer, and a lower substrate temperature offers wider choice of substrates and reduced thermal stress Diserens, *et al*. 1998; and Zhang, *et al*. 2003)**.**

In this paper we report the use of ionized magnetron sputter deposition (IMSD)

to prepare *nc*-TiN/*a*-SiN*x* films and the correlation between film properties and preparation conditions. Co-sputtering of single element targets allows an easy adjustment of the stoichiometry of the deposited films, and ion assisted deposition provides good control of energetic ion bombardment during film growth, in terms of both flux and energy (Chiu, *et al.* 2002; Chiu, *et al.* 1999; and Rossnagel, *et al*. 1993)**.** An increase in surface mobility provided by this bombardment can enhance the segregation of nanocrystalline TiN in the amorphous silicon nitride matrix, leading to improved mechanical properties (Diserens, *et al.* 1998; and Vaz, *et al.* 2001)**.**

MEASUREMENT OF HARDNESS

Hardness is defined as the resistance of a given material against plastic deformation. The materials' ability to resist deformation under isostatic pressure is called theoretical hardness. It is known that the theoretical hardness is proportional to the reciprocal value of bulk modulus B where B can be found from the relationship between the binding energy (E_b) and the bond distance (a) at equilibrium position as shown in equation(1) (Niederhofer, *et al.* 1999). Therefore the materials with a short bond distance and with high bond energy can result in a high theoretical hardness.

$$B = \frac{d^2 E_b}{da^2} \qquad \text{----------(1)}$$

The practical hardness of materials can be determined by the microstructure that hinders the multiplication and movement of the dislocations as well as the growth of the microcracks. It is usually found to be smaller than the theoretical one and can be calculated from the applied load used for indentation and the measured plastic deformation area.

For the works that require a small load such as thin films, a nanoindentation technique is selected. Figure 1 shows the typical indentation load-displacement curves measured by nanoindentation. L_{max} is a maximum applied load, mN, and d_{max} is the maximum penetration depth of the diamond indenter. Areas a and b represent plastic deformation and elastic recovery respectively.

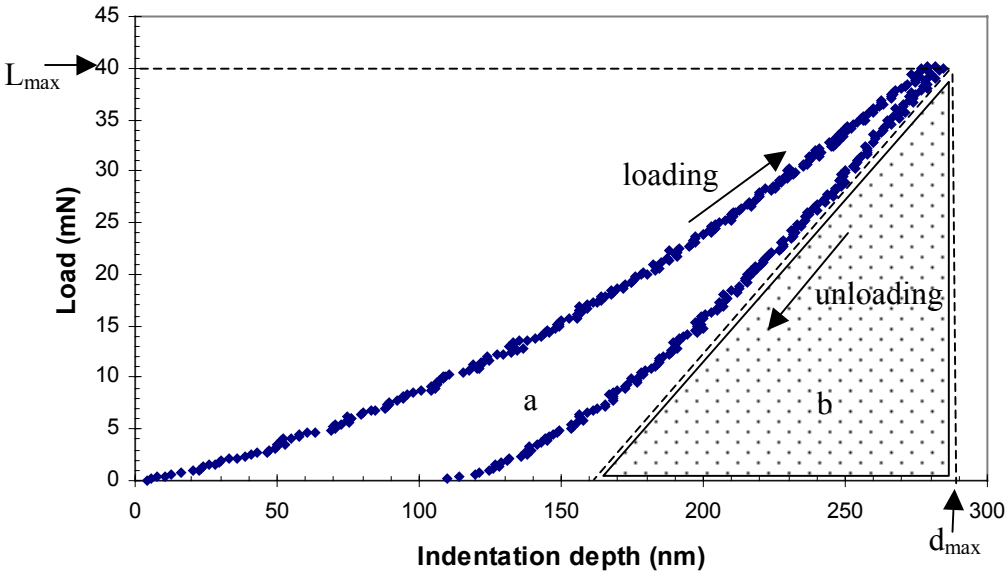

Figure 1 Typical load/unloading curves of the nanocomposite TiN/*a*-SiN$_x$ films.

EXPERIMENTAL METHODOLOGY

Ti-Si-N films were deposited on 5mm x 10mm R-plane sapphire ($1\bar{1}02$) and fused silica substrates by IMSD: a schematic diagram is shown in Figure 2. The 55mm x 35mm x 2mm Ti (99.96%) and Si (99.999%) targets were attached to the dc magnetrons, and the stoichiometry, $Ti_{(1-x)}:Si_x$ (where x is the atomic fraction of Si : x = Si/[Ti+Si]), could be precisely controlled with the power to each target. A three-turn rf coil placed between targets and substrates generated an inductively coupled plasma. By electrically isolating the substrate holder from the chamber, the substrates could be electrically floating, earthed or biased. Therefore, the ion flux (mA cm^{-2}) and ion incident energy (eV) at the substrate surface could be controlled by the rf power and dc substrate bias, respectively. The Ti target power was typically set at 5.2 W/cm^2 and the Si target power was varied (1.55-2.60 W/cm^2).

The base pressure in the deposition chamber was 10^{-8} Pa, and the depositions were carried out in 1.4 Pa Ar/N_2 (50:50): the gases both (99.9999%) were pre-mixed in a reservoir and bled into the system via a leak valve. The gas flow rate and pressure were controlled by setting the leak and gate valve to the main pump. The target to substrate distance was fixed at 40 mm. The substrates rested on a platinum strip heater. The heater temperature was measured with an optical pyrometer and the substrate temperature (T_{sub}) was estimated using previous calibrations. Targets were pre-sputtered for 15 minutes prior to film growth, with a shutter placed in front of the substrates.

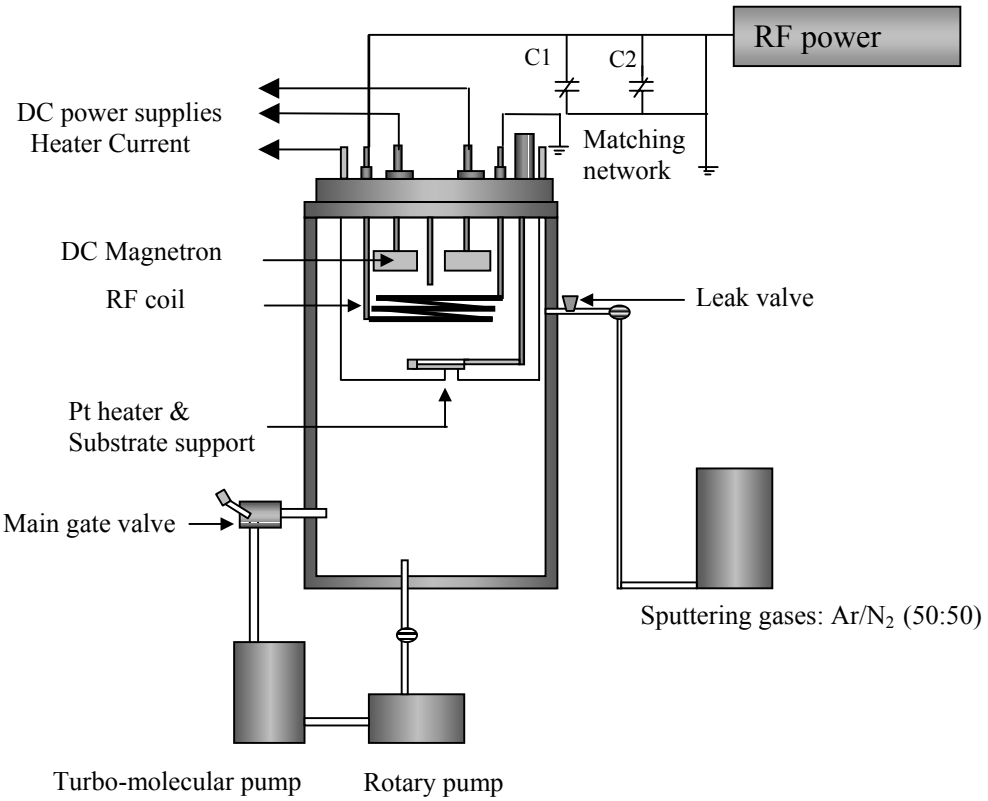

Figure 2 Schematic of the IMSD system

Film stoichiometry was determined by energy dispersive X-ray analysis (EDAX) in a scanning electron microscope (JEOL). The structure, texture, and grain size of the films were determined by X-ray diffraction (XRD), (PHILIPS/XPERT diffractometer), using CuKα radiation in a θ-2θ configuration. To

simplify the presentation of the XRD analysis we illustrated results from films on fused silica substrates, which show no X-ray peaks themselves. The structural characteristics of films on r-plane sapphire were identical.

The crystallite domain size was calculated from the width of the XRD peaks, assuming that they are free from non-uniform strains, using the Scherrer formula.

$$L = \frac{0.9\lambda}{(B * \cos\theta)}$$

Where L is the average crystallite domain size perpendicular to the reflecting planes, λ is the X-ray wavelength, B is the full width at half maximum (FWHM), and θ is the diffraction angle. To eliminate additional instrumental broadening the FWHM was corrected, using the FWHM from a large grained Si sample.

$$B_{corrected} = (FWHM^2_{sample} - FWHM^2_{Si})^{\frac{1}{2}}$$

This modified formula is valid only when the crystallite size is smaller than 100 nm (Boulch, *et al.* 2001).

Film thickness was measured from a step on a masked substrate using a profilometer (Rank Taylor-Hobson). The deposition rate was 25 nm min^{-1} and films were typically 3-3.5 μm thick. Films hardness, H, was measured with nanoindentation (Nanotest 600, Micro Materials Ltd, Wrexham, UK, fitted with Berkovich indenter: a three-sided pyramid with the same area-to-depth ratio as a Vickers indenter). The intrinsic mechanical properties of these films were measured at indentation depths between 200nm and 330nm, which is less than 10% of the film thickness. The influence of the mechanical properties of the substrate on the measurement is therefore avoided. A test load of 30 mN was typically used and the loading and unloading speed was kept at 0.8 nm s^{-1}. The Oliver-Pharr method was used to analyze the loading and unloading curves. To minimize creep and thermal drift effects the hold period was kept at 10 s at maximum depth and 60 s during unloading at 20% of the maximum load.

RESULTS AND DISCUSSION

Figure 3 shows a comparison between the loading and unloading curves of TiN and high hardness *nc*-TiN/*a*-SiN$_x$ films. Figure 4 shows how homogenous the coating is. The uniform coating can be determined by the reproducibility of five indentations at different locations.

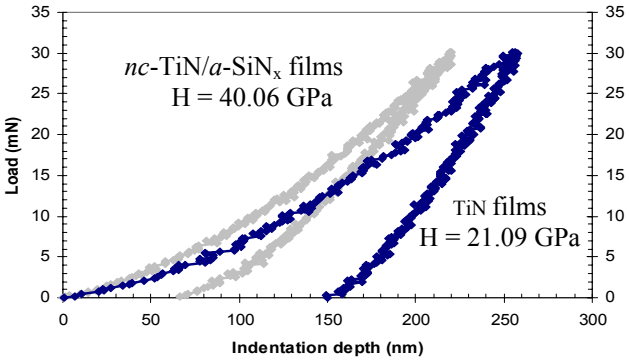

Figure 3 The indentation load-displacement curves of TiN and high hardness *nc*-TiN/*a*-SiN$_x$ films (deposited using IMSD under different conditions).

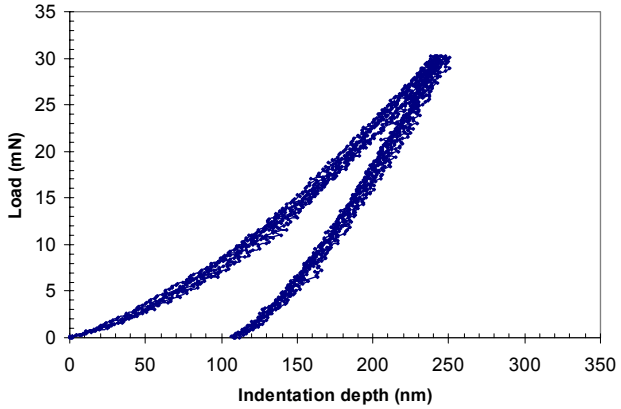

Figure 4 Five indentation load-displacement curves of *nc*-TiN/*a*-SiN$_x$ films ($Ti_{0.86}$:$Si_{0.14}$, T_{sub}= 250^{o}C, 80W rf power, -80V Bias) at different locations.

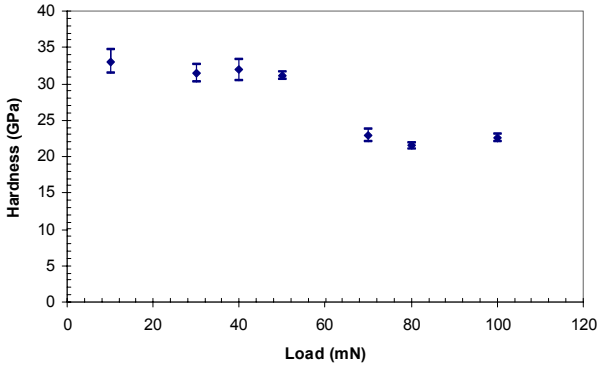

Figure 5 The relationship between hardness and applied load of a 3.5 μm thick *nc*-TiN/*a*-SiN_x film ($Ti_{0.78}$:$Si_{0.22}$, T_{sub}= 250°C, 50W rf power, -80V Bias)

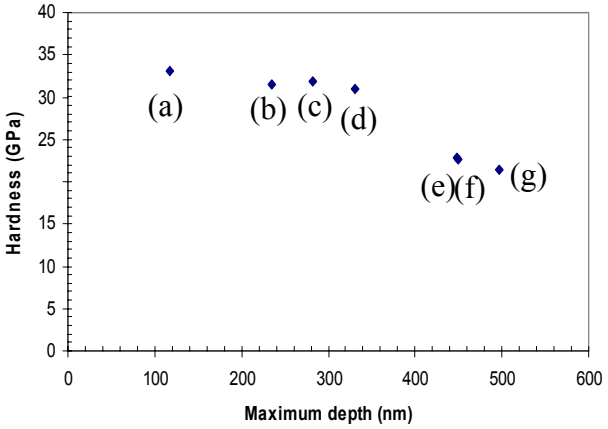

Figure 6 The relationship between hardness and maximum indentation depth of a 3.5 μm thick *nc*-TiN/*a*-SiN_x film at (a) 10mN, (b) 30mN, (c) 40mN, (d) 50mN, (e) 70mN, (f) 80mN and (g) 100mN load ($Ti_{0.78}$:$Si_{0.22}$, T_{sub}= 250°C, 50W rf power, -80V Bias)

Figure 5 shows the relationship between hardness and applied load and Figure 6 shows the relationship between film hardness and the maximum indentation depth at various applied load. The results show that at applied loads below 70 mN the maximum indentation depth remains less than 10% of the film thickness. Therefore the influence of the substrate on the measured film hardness can be eliminated.

At applied loads of 70, 80 and 100 mN the maximum indentation depth is more than 10% of the film thickness. The hardness of the films is decreased by the influence of the sapphire substrate (the hardness of the sapphire substrate, H=20GPa).

The effect of the silicon content on the hardness of the films is shown in Figure 7. At constant experimental conditions (50W rf power, -80V substrate bias, and 250°C substrate temperature) the hardness increased with increasing Si content, reaching a maximum

(at $x \cong 0.18$) and then decreases. Figure 8 shows the XRD spectra of *nc*-TiN/*a*-SiN_x films with different Si contents. Only diffraction peaks assigned to the crystalline TiN phase were observed, without appearance of crystalline Si, Si_3N_4, or phases of titanium silicide. This implies that silicon is present in an amorphous phase of either silicon nitride or silicon. These findings are in agreement with earlier reports (Diserens, *et al*. 1998; Meng, *et al.* 2003; Niederhofer, *et al.* 1999; Vaz, *et al.* 1999; and Zhang, *et al*. 2003). Pure TiN deposited under identical conditions exhibits a pronounced (111) texture with relatively sharp peaks indicative of a grain size of 29 nm. With increasing silicon content the orientation is gradually changed from (111) to (200) with broadening of the peaks. The calculated crystallite size decreased to less than 10 nm for $x \geq 0.17$.

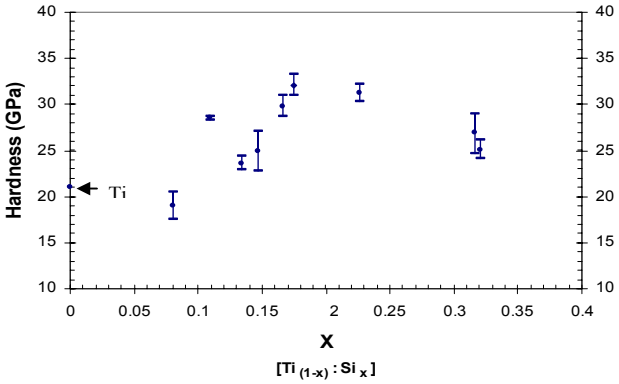

Figure 7 The relationship between hardness and Si content in *nc*-TiN/*a*-SiN_x films (T_{sub} =250°C, 50W rf power, and -80 V bias)

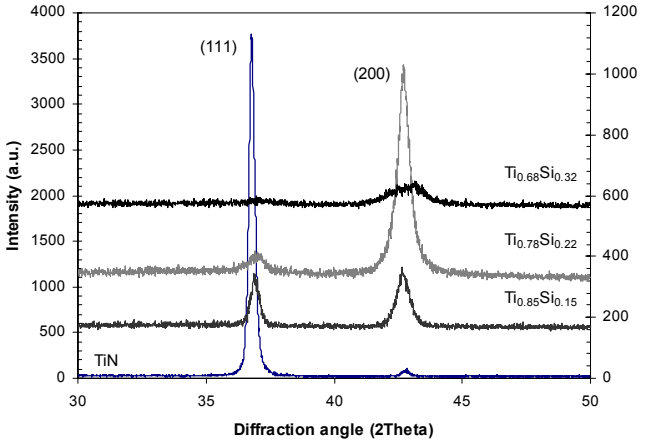

Figure 8 XRD spectra of *nc*-TiN/*a*-SiN$_x$ films with varying Si content (T_{sub} =250^{o}C, 50W rf power, and -80V bias)

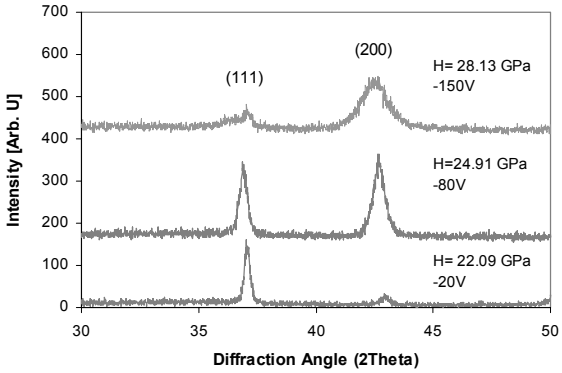

Figure 9 The XRD spectra of *nc*-TiN/*a*-SiN$_x$ films ($Ti_{0.86}$:$Si_{0.14}$, T_{sub} =250°C, and 50W rf power) with different negative substrate bias voltages, V= -20, -80, and -150 V

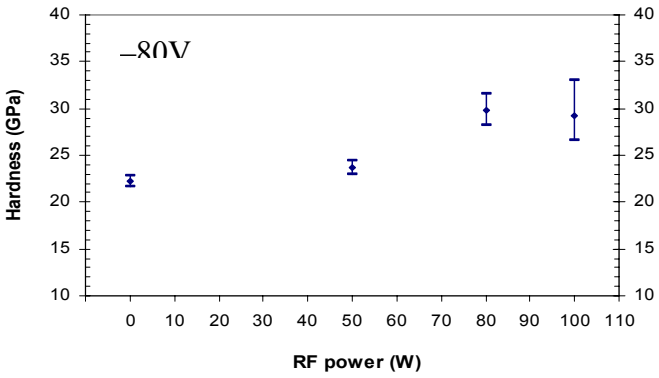

Figure 10 The effect of rf power on the hardness of *nc*-TiN/*a*-SiN$_x$ films ($Ti_{0.86}$:$Si_{0.14}$ and T_{sub} =250^{o}C, –80V bias)

Figure 9 and 10 show that film hardness increases with increasing negative bias voltage and rf power. This is because the segregation of phases can be enhanced by the increase of adatom surface mobility provided by increased temperature and/or energetic bombardment. The results suggest that sufficient energy was delivered during film growth at –150V applied bias and 50W rf power, to lead to a hardness significantly above that of polycrystalline TiN. With an rf power of 100 W, bias = –150V, a $Ti_{0.88}$:$Si_{0.12}$ film showed a hardness of 40GPa

XRD analysis also confirmed that the film microstructure changed from (111) to (200), the preferred orientation, with smaller crystallite size, on increasing negative substrate bias. However at negative bias voltage ≥ -200V we observed that the surface of the films became rough, and there were indications of high compressive stress (some buckling and peeling), Figure 11.

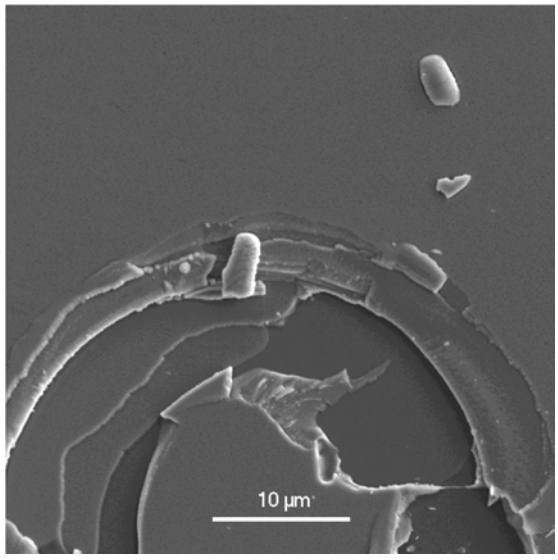

Figure 11 SEM image of the surface of the film deposited at negative bias above 200 V. There is an indication of high compressive stress.

CONCLUSION

Nanocomposite TiN/SiN$_x$ films were depsosited by using theIMSD technique. The

hardness of the films was measured using nanoindentation and the coatings showed high hardness at low deposition temperatures through bombardment-induced phase segregation. The results show the effects of ion flux and energetic bombardment on the properties of the films. Ion bombardment influences the texture, structure, and crystallite domain size and therefore mechanical properties of the films. EDAX and XRD analysis indicates the formation of an amorphous phase and nanocrystalline TiN.

REFERENCES

Boulch, F., Schouler, M-C., Donnadieu, P., Chaix, J-M. and Djurado, E. 2001. Domain size distribution of Y-TZP nano-particles using XRD and HRTEM. *Image Anal Stereol.* **20** : 157-161.

Chiu, K-F. and Barber, Z. H. 2002. Plasma characterization of ionized physical vapor deposition system. *J. Appl. Phys.* **91** : 1797 – 1803.

Chiu, K-F., Blamire, M. G. and Barber, Z. H. 1999. Microstructure modification of silver films deposited by ionized magnetron sputter deposition. *J. Vac. Sci. Technol. A.* **17(5)** : 2891.

Diserens, M., Patscheider, J. and Levy, F. 1998. Improving the properties of titanium nitride by incorporation of silicon. *Surf. Coat. Technol*. **108-109** : 241-246.

Diserens, M., Patscheider, J. and Levy, F. 1999. Mechanical properties and oxidation resistance of nanocomposite TiN-SiN_x physical-vapor-deposited thin films. *Surf. Coat. Technol*. **120-121** : 158-165.

Jedrzejowski, P., Klemberg-Sapieha, J. E. and Martinu, L. 2003. Relationship between the mechanical properties and the microstructure of nanocomposite TiN/SiN1.3 coatings prepared by low temperature plasma enhanced chemical vapor deposition. *Thin Solid Films*. **426** : 150-159.

Kim, S. H., Kim, J. K. and Kim, K. H. 2002. Influence of deposition conditions on the microstructure and mechanical properties of Ti-Si-N films by Dc reactive magenetron sputtering. *Thin Solid Film.* **420-421** : 360-365.

Martin, P. J. and Bendavid, A. 2003. Properties of $Ti_{1-x}Si_xN_y$ films deposited by concurrent cathodic arc evaporation and magnetron sputtering. *Surf. Coat. Technol.* **163-164** : 245-250.

Meng,W. J., Zhang, X. D., Shi, B., Jiang, J. C., Rehn, L. E., Baldo, P. M. and Tittsworth, R. C. 2003. Structure and mechanical properties of Ti-Si-N ceramic nanocomposite coatings. *Surf. Coat. Technol.* **163-164** : 251-259.

Musil, J. and Vlcek, J. 2001. Magnetron sputtering of hard nanocomposite coating and their properties. *Surf. Coat. Technol.* **142-144** : 557-566.

Neiderhofer, A., Bolom, T., Nesladek, P.,Moto, K., Patil, D. S. and Veprek, S. 2001. The role of percolation threshold for the control of hardness and thermal stability of super- and ultrahard nanocomposites. *Surf. Coat. Technol.* **146-147** : 183-188.

Niederhofer, A., Nesladek, P., Mannling, H.-D., Moto, K., Veprek, S. and Jilek, M. 1999. Structural properties, internal stress and thermal stability of nc-TiN/-Si_3N_4, nc-TiN/$TiSi_x$ and nc-$(Ti_{1-y}Al_ySi_x)N$ superhard nanocomposite coatings reaching the hardness of diamond. *Surf. Coat. Technol.***120-121** : 173-178.

Patscheider, J., Shizhi, L. and Veprek, S. 1996. Plasma induced deposition titanium nitride from TiCl4 in a direct

current glow discharge. *Chem. Plasma Proc*. **16** : 341.

Rebouta, L., Travares, C. J., Aimo, R., Wang, Z., Pischow, K., Alves, E., Rojas, T. C., Odriozola, J. A. 2000. Hard nanocomposite Ti-Si-N coatings prepared byDC reactive magenetron sputtering. *Surf. Coat.Technol.* **133-134** : 234-239.

Rossnagel, S. M. and Hopwood, J. 1993. Magnetron Sputter Deposition with levels of metal ionization. *Appl. Phys. Lett.* **63** : 3285-3287.

Vaz, F., Rebouta, L., Goudeau, P., Pacaud, J., Garem, H., Rivere, J. P., Cavaleiro, A. and Alves, E. 2000. Characterisation of $Ti_{1-x}Si_xN_y$ nanocomposite films. *Surf. Coat. Technol.* **133-134** : 307-313.

Vaz, F., Rebouta, L., Goudeau, Ph., Girardeau, T., Pacaud, J., Rivere, J. P. and Traverse, A. 2001. Structure transitions in hard Si-baed TiN coatings: the effect of bias voltage and temperature. *Surf. Coat. Technol.* **146-147** : 274-279.

Vaz, F., Rebouta, L., Almeida, B., Goudeau, P., Pacaud, J., Rivere, J. P. and Sousa, J. B. E. 1999. Structure analysi of $Ti_{1-x}Si_xN_y$ nanocomposite films prepared by reactive magnetron sputtering. *Surf. Coat. Technol.* **120-121** : 166-172.

Veprek, S. 1999. The search for novel, superhard materials. *J. Vac. Sci. Technol. A*. **17(5)** : 2401-2420.

Zhang, S., Sun, D., Fu, Y. and Du, H. 2003. Recent advances of superhard nanocomposite coatings: a review. *Surf. Coat. Technol.* **167** : 113-119.

(Revised version accepted October 28 , 2003)